Mechanism and Machine Theory 197 (2024) 105652

Contents lists available at ScienceDirect

Mechanism and Machine Theory

journal homepage: www.elsevier.com/locate/mechmt

Research paper

# Full pose measurement system for industrial robots kinematic calibration based on a sensorized spatial linkage mechanism

Monica Tiboni [a,*], Giovanni Legnani [a], Roberto Bussola [a], Diego Tosi [b]

[a] Department of Mechanical and Industrial Engineering, University of Brescia, via Branze, 38, 25123 Brescia, Italy
[b] Crosstech srl, via Triumplina, 88, 25123 Brescia, Italy

ARTICLE INFO

*Keywords:*
Pose measuring
Kinematic calibration
Industrial robots
Linkage spatial mechanism

ABSTRACT

This paper presents a low-cost pose measuring device capable of simultaneously measuring all six coordinates (3 translations and 3 rotations) of a rigid body with respect to a given reference frame. The proposed system consists of a mechanical chain of rigid bodies and two encoders. The mechanism is a spatial four-bar linkage system with a symmetrical Revolute-Spherical-Spherical-Revolute (RSSR) kinematic structure, where two encoders measure the rotation of the revolute joints. The mechanism is investigated theoretically and solved kinematically using a numerical estimation method. The uncertainty of the pose determination, caused by the repeatability of the sensors, is estimated, as well as the achievable measurement range. A low uncertainty is achieved by a suitable design of the proposed kinematic chain. The mechanism is easy to realize with low tolerances and the correct definition of the length of the links allows a quite large workspace. The system can be profitably used in the calibration of robots or multi-axis machine tools where the actual pose of the gripper or spindle must be measured over the workspace of the machine. An experimental prototype is described, and the first experimental results are reported.

## 1. Introduction

Robotic manipulators are employed in the industrial sector in many applications. Accuracy and repeatability of a robot are very important features, which significantly influence performance in an industrial environment [1,2]. Accuracy is more relevant than repeatability when the robot is used in advanced applications, e.g. micro-assembly operations, robot-based measurement, welding tasks, and off-line programming. The repeatability of industrial robots is typically very good, on the order of tenths of mm (even up to 0.02 mm), while the accuracy is not so good. The accuracy can sometimes even be 20 mm [3].

Inaccuracies of industrial robots are mainly related to structural mechanics, as a matter of fact about 90% of the total positioning error is caused by geometrical errors, i.e. link lengths, joint offsets, and link twist angles [4–7].

Zhong [8] and Shiakolas [9] argue that among these, joint offsets mainly affect accuracy. Due to manufacturing errors, different exemplars of the same robot model usually have differences in structural parameters, such as the offsets of the joints, which can be influenced by the assembly or replacement of motors and encoders. The mathematical model within the robot controller assumes that the links of a robot have nominal length values so that the same values are taken into account in the model of another robot of the same type. Similarly, this happens for the relative orientations of the joint axes. Unfortunately, this is not the case. The positioning errors of the end-effector can also be caused by the imperfect assembly of different links and result from the displacement and/or

* Corresponding author.
*E-mail addresses:* monica.tiboni@unibs.it (M. Tiboni), giovanni.legnani@unibs.it (G. Legnani), roberto.bussola@unibs.it (R. Bussola), diego.tosi@crosstech.it (D. Tosi).

https://doi.org/10.1016/j.mechmachtheory.2024.105652
Received 16 January 2024; Received in revised form 27 February 2024; Accepted 13 April 2024
Available online 22 April 2024

rotation of the frames connected to different elements that are normally assumed to be aligned with each other. In addition, other factors such as thermal expansion, clearances in mechanical couplings, joint compliance, structural deformations, etc. can also play a role. All these causes of inaccuracy lead to a deviation between the theoretical and the real position of the robot if they are not taken into account in the model used by the robot controller to calculate the kinematics. Therefore, inaccurate values in the kinematic parameters specified in the robot controller are the main cause of pose inaccuracies.

In applications for which high accuracy is required, the implementation of robot calibration procedures is essential. Many calibration methods have been developed for estimating and compensating for pose errors [1,10–16]. Most of these methods require the measurement of the actual gripper pose of the robot at different positions in the workspace. The adopted measurement techniques are classified into open-loop and closed-loop [6]. Open-loop methods use external measuring devices, such as laser tracking systems [17,18], a laser displacement meter [17,19], Coordinate Measurement Machines (CMMs) [20], Computer Numerical Controlled (CNC) machines [21], optical sensors (mirrors and laser point sensors, interferometers) [22–24], cameras [25,26], inclinometers or accelerometers [27–29], theodolites [30–32], wire potentiometers [3,33], instrumented ballbar [34], telescopic ballbar [35] and many others.

The second class is related to devices that form a closed kinematic chain when coupled with the robot, by applying physical constraints to the robot Tool Center Point (TCP) [8,36–39].

Hollerbach and Wampler in [35] presented a taxonomy of kinematic calibration methods for which all methods are unified in the definition of kinematic loop methods: all methods are considered closed-loop, and in open-loop methods the measurement system is considered to form a joint.

Usually, six coordinates are measured, three translational coordinates for the position and three rotational coordinates for the orientation, otherwise in a limited number of cases only the position is measured [40]. In practice, partial pose information is often used, which provides one- to five-dimensional measurements instead of full pose information. In general, the low-dimensional measurement is more attractive as the set-up of the calibration experiment is simpler.

Most of the adopted sensors can only detect a portion of the body's pose. For example, a double ball bar system measures one coordinate per pose (the distance between the centers of the balls), inclinometers can only measure two angles (tilt and rotation) and laser trackers the three translations of a body point.

The complete measurement of body pose is possible with the help of dimes, cameras, or a combination of different sensors. In general, the most accurate measurement systems are very expensive and often not easy to install and use. A large measurement range is another desirable feature that is difficult to achieve.

A monocular camera-based method for kinematic calibration is presented by Boby in [26]. The TCP pose is not measured directly, but the 2-D images captured by a monocular camera mounted on the end-effector are used to measure errors, and corrections in the parameters space are made to correct errors detected in 2-D images. The results obtained with random measurements showed that the average accuracy decreased from 4.67 mm to 3.07 mm, a positive result, but still far from the result of 0.9 mm achieved with a laser tracker system.

Filion et al. [41] investigate the possible use of a commercially available portable photogrammetry system (the MaxSHOT 3D) in the calibration of industrial robots. The obtained accuracy after kinematic calibration (0.439 maximum and 0.197 mean) is comparable with that obtained with the FARO laser tracker (0.356 maximum and 0.147 mean).

The development of a measuring system based on wire sensors and its application to an anthropomorphic robot with six degrees of freedom led to an accuracy of around 2 mm [33].

Driels et al. [20] used a coordinate measuring machine (CMM) to measure the center positions of five spheres placed on specially designed end effectors and achieved an accuracy in the order of 0.3 mm with kinematic calibration.

Nubiola et al. [35] presented a method to fully measure the posture of robotic end-effectors using a single telescopic ball bar and two planar fixtures. Each fixture carries three magnetic cups located at the corners of an equilateral triangle. This device has a hexapod geometry, it is therefore an extension of a known approach using a hexapod (a Stewart-Gough platform) with telescopic legs. The positional accuracy of the device is in the range of $\pm 0.003$mm, making it suitable for measuring the pose accuracy and repeatability of industrial robots and even for their calibration, and enables the acquisition of more than fifty poses under static conditions.

Besnard et al. [42] developed a method for the kinematic calibration of parallel robots with six degrees of freedom using two inclinometers. They achieved an accuracy of 0.4 mm in the simulation.

This article presents a system for measuring pose, based on a spatial four-bar linkage mechanism with $RSSR$ chain (R=rotational linkage, S=spherical linkage), in which the pose is estimated by measuring the rotation of the two rotational joints.

This class of mechanisms has been analyzed in detail by several researchers. The motion analysis was studied in [43–48], the synthesis and motion generation performances are the most analyzed points [49–54], but has never been used as a 3D measurement system.

In Section 2 the considered mechanism is described (Section 2.1), and the pose estimation approach is explained (Section 2.2). After a brief description of the notation used, the kinematics of the system and the procedure for pose estimation in analytical form are developed. Section 2.3 examines the uncertainty of the pose estimation. The results of experiments performed on a prototype of the mechanism are presented in Section 3. The design solution is described in Section 3.1, and 3.4 compares them with the theoretical ones (Section 3.3). In Section 4 the conclusions are drawn.

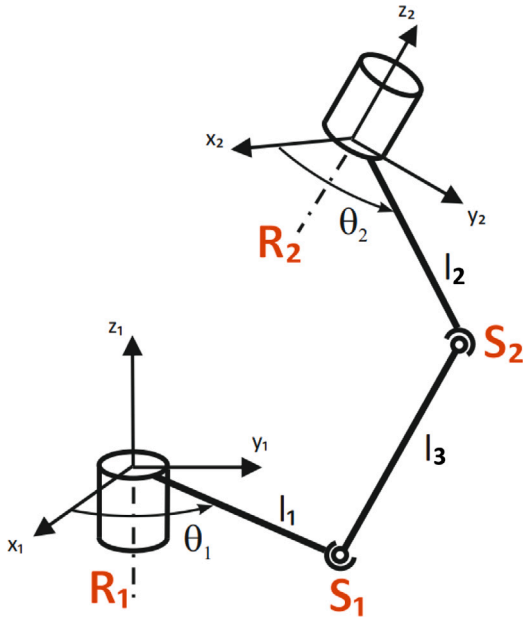


**Fig. 1.** Kinematic scheme of the four-bar linkage measurement system.

## 2. The considered linkage-based measuring mechanism

### 2.1. Spatial four-bar linkage measuring mechanism description

The proposed measurement system consists of a symmetrical serial chain with RSSR structure, i.e. with three links connected respectively by a revolute joint, two ball joints and a revolute joint, as shown in Fig. 1.

When the pose of a body is measured, two reference frames are implicitly defined: one is embedded in the body and moves with it (the "mobile" frame), and the other is fixed to the ground or, more generally, to the base of the measuring system (the "reference frame"), as visible in Fig. 1.

The first revolute joint is connected to the reference frame and the last one is connected to the body (the gripper) whose position is to be measured (Fig. 2).

By assigning an arbitrary pose to the body, the system forms a spatial joint with four rods. An important feature of the mechanism is that the serial chain has an internal degree of freedom (DoF). This means that the coordinate of a joint can assume any value (within a defined range) when the pose of the first and last frame of the chain is determined. For example, one of the two revolute joints can rotate freely and the other joints move uniformly.

By simultaneously measuring the rotations of the two revolute joints $\theta_1$ and $\theta_2$ in several positions (at least six), the position of the movable frame in relation to the fixed frame can be estimated.

For better clarification, the reference frame and the moving frame can be considered as the fixed and moving base of a virtual parallel kinematic machine (PKM), whose legs are the $SS$ links of the four-bar linkage in different positions (Fig. 3). In this virtual PKM, the ball joints at the bases are placed on circles and all legs have the same length. By simultaneously measuring the rotations of the pivot points and knowing the dimensions of the links, the position of the spherical joints of the fixed and movable base can be calculated. The pose of the moving base can be calculated if there are at least six positions of the mechanism forming a PKM in a non-singular configuration.

Depending on the selected pose, neither, one or both of the revolute joints can perform a complete rotation (see Section 2.2). Of course, more than six measurements can be performed for the same pose within the allowed ranges, which avoids the singular configuration and greatly reduces the uncertainty of the estimation (see Section 2.3).

### 2.2. Pose estimation approach

#### 2.2.1. Notation

Table 1 summarizes the notation used to describe the spatial four bar linkage shown in Fig. 1.

$x_1$ $y_1$ $z_1$ and $x_2$ $y_2$ $z_2$ denote the axes of the reference frame and the moving frame, respectively. $\theta_1$ and $\theta_2$ are the angles of rotation of the two revolute joints $R_1$ and $R_2$. $l_1$ $l_2$ $l_3$ are the lengths of the three links.

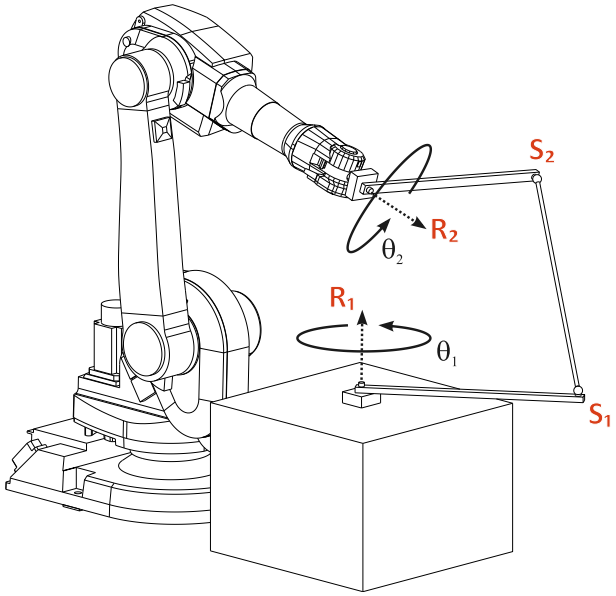


**Fig. 2.** Use of the spatial linkage to measure the pose of an industrial robot with serial kinematic chain.

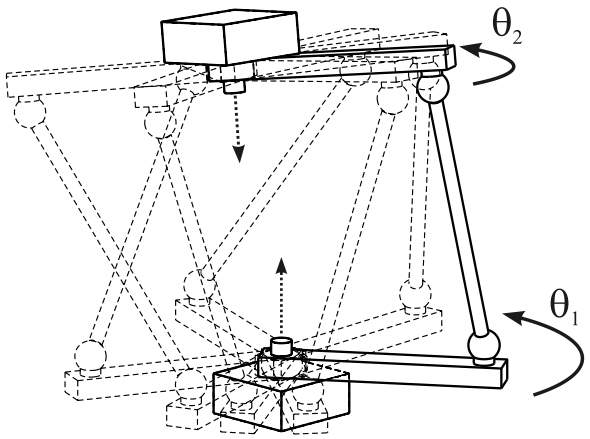


**Fig. 3.** Definition of a virtual parallel kinematic machine (PKM) by the movement of the four-bar linkage.

**Table 1**
Notation used to describe the spatial four-bar linkage.

| | |
|---|---|
| $x_1\ y_1\ z_1$ | Reference frame |
| $x_2\ y_2\ z_2$ | Mobile frame |
| $\theta_1$ | Rotation angle of the revolute joint $R_1$ |
| $\theta_2$ | Rotation angle of the revolute joint $\mathbb{R}_2$ |
| $l_1\ l_2\ l_3$ | Links lengths |
| $\mathbf{S_1}\ \mathbf{S_2}$ | Spherical joints |
| $\mathbf{R_1}\ \mathbf{R_2}$ | Revolute joints |

### 2.2.2. Constraint equation

By assigning a pose to the moving frame {2}, the mechanism still has a DoF with respect to the reference frame {1}, i.e. the values of the rotation angles $\theta_1$ and $\theta_2$ cannot assume arbitrary values, but must fulfill a constraint equation, the so-called closure equation.

To avoid the singularities associated with the choice of a particular set of rotation angles, the relative pose of the frame {2} with respect to {1} was described with a general roto-translation transformation matrix **T** (Eq. (1)).

$$\mathbf{T} = \left[\begin{array}{ccc|c} r_{11} & r_{12} & r_{13} & t_x \\ r_{21} & r_{22} & r_{23} & t_y \\ r_{31} & r_{32} & r_{33} & t_z \\ \hline 0 & 0 & 0 & 1 \end{array}\right] = \left[\begin{array}{ccc|c} & \mathbf{R} & & \overline{\mathbf{T}} \\ \hline 0 & 0 & 0 & 1 \end{array}\right] \tag{1}$$

where **R** is a rotation matrix, ans so it is orthogonal.

The spatial position of the two spherical joints $\mathbb{S}_1$ and $\mathbb{S}_2$ can be computed by using homogeneous coordinates as follows:

$$S_1 = \begin{bmatrix} l_1\cos(\theta_1) \\ l_1\sin(\theta_1) \\ 0 \\ 1 \end{bmatrix} S_2 = \begin{bmatrix} l_2(r_{11}\cos(\theta_2) + r_{12}\sin(\theta_2)) + t_x \\ l_2(r_{21}\cos(\theta_2) + r_{22}\sin(\theta_2)) + t_y \\ l_2(r_{31}\cos(\theta_2) + r_{32}\sin(\theta_2)) + t_z \\ 1 \end{bmatrix} \tag{2}$$

The constraint equation Eq. (3) is obtained by setting the distance between the two centers of the ball joints equal to $l_3$.

$$\begin{aligned} &f(\mathbf{T},\theta_1,\theta_2) = (S_1 - S_2)^t(S_1 - S_2) - l_3^2 = \\ &= (l_2(r_{11}c_{\theta_2} + r_{12}s_{\theta_2}) + t_x - l_1c_{\theta_1})^2 + (l_2(r_{21}c_{\theta_2} + r_{22}s_{\theta_2}) + \\ &t_y - l_1s_{\theta_1})^2 + (l_2(r_{31}c_{\theta_2} + r_{32}s_{\theta_2}) + t_z)^2 - l_3^2 = 0 \end{aligned} \tag{3}$$

where:

$$s_{\theta_1} = \sin(\theta_1) \quad c_{\theta_1} = \cos(\theta_1) \quad s_{\theta_2} = \sin(\theta_2) \quad c_{\theta_2} = \cos(\theta_2) \tag{4}$$

### 2.2.3. Solutions of the constraint equation

If the pose matrix **T** is known, the constraint equation (Eq. (3)) is solved by calculating the angle $\theta_1$ in relation to $\theta_2$, or vice versa. To solve the constraint Eq. (3) with respect to $\theta_2$, all terms containing $\sin(\theta_2)$ and $\cos(\theta_2)$ can be collected, as in Eq. (5).

$$(k_1\cos(\theta_2) + k_2)\sin(\theta_2) + k_3\cos(\theta_2)^2 + k_4\cos(\theta_2) + k_5 = 0 \tag{5}$$

where

$$\begin{aligned} k_1 &= 2l_2^2\left(r_{11}r_{12} + r_{21}r_{22} + r_{31}r_{32}\right) \\ k_2 &= -2l_1l_2\left(r_{12}\cos(\theta_1) + r_{22}\sin(\theta_1)\right) + \\ &\quad 2l_2\left(r_{12}t_x + r_{22}t_y + r_{32}t_z\right) \\ k_3 &= l_2^2\left(r_{11}^2 + r_{21}^2 + r_{31}^2 - r_{12}^2 - r_{22}^2 - r_{32}^2\right) \\ k_4 &= -2l_1l_2\left(r_{21}\sin(\theta_1) + r_{11}\cos(\theta_1)\right) \\ &\quad +2l_2\left(r_{11}t_x + r_{21}t_y + r_{31}t_z\right) \\ k_5 &= t_x^2 + t_y^2 + t_z^2 + l_1^2 + l_2^2\left(r_{12}^2 + r_{22}^2 + r_{32}^2\right) - l_3^2 + \\ &\quad -2l_1\left(t_x\cos(\theta_1) + t_y\sin(\theta_1)\right) \end{aligned} \tag{6}$$

Considering that **R** is an orthogonal matrix (thus its columns are unitary and mutual orthogonal), for all possible sets of angular coordinates, $r_{11}^2 + r_{21}^2 + r_{31}^2 - r_{12}^2 - r_{22}^2 - r_{32}^2 = 0$, $r_{11}r_{12} + r_{21}r_{22} + r_{31}r_{32} = 0$, and $r_{12}^2 + r_{22}^2 + r_{32}^2 = 1$. It follows that:

$$\begin{aligned} &k_1 = 0, \\ &k_3 = 0, \\ &k_5 = t_x^2 + t_y^2 + t_z^2 + l_1^2 + l_2^2 - l_3^2 - 2l_1(t_y\sin(\theta_1) + t_x\cos(\theta_1)) \end{aligned} \tag{7}$$

then Eq. (5) can be simplified as

$$k_2\sin(\theta_2) + k_4\cos(\theta_2) + k_5 = 0 \tag{8}$$

The previous equation has 2 solutions:

$$\begin{aligned} &\theta_{2A},\theta_{2B} = \\ &atan2((k_4(k_5k_4 \pm K_1)/K_2 - k_5)/k_2, -(k_5k_4 \pm K_1)/K_2), \\ &K_1 = \sqrt{k_4^2k_2^2 + k_2^4 - k_2^2k_5^2}, \\ &K_2 = k_4^2 + k_2^2 \end{aligned} \tag{9}$$

The solution of the constraint equation Eq. (3) with respect to $\theta_1$ results in the Eq. (10).

$$v_1\sin(\theta_1) + v_2\cos(\theta_1) + v_3 = 0 \tag{10}$$

where

$$\begin{aligned} v_1 &= -2l_2r_{21}c_{\theta_2}l_1 - 2l_2r_{22}s_{\theta_2}l_1 - 2t_yl_1, \\ v_2 &= -2l_2r_{12}s_{\theta_2}l_1 - 2l_2r_{11}c_{\theta_2}l_1 - 2t_xl_1, \\ v_3 &= l_2^2(r_{11}^2 + r_{21}^2 + r_{31}^2 - r_{12}^2 - r_{22}^2 - r_{32}^2)c_{\theta_2}^2 + \\ &\quad +2l_2^2(r_{11}r_{12} + r_{21}r_{22} + r_{31}r_{32})s_{\theta_2} + \\ &\quad +2l_2\left(r_{11}t_x + r_{21}t_y + r_{31}t_z\right)c_{\theta_2} + \\ &\quad +2l_2\left(r_{12}t_x + r_{22}t_y + r_{32}t_z\right)s_{\theta_2} + t_x^2 + t_y^2 + t_z^2 + \\ &\quad +l_1^2 + l_2^2(r_{12}^2 + r_{22}^2 + r_{32}^2) - l_3^2 \end{aligned} \tag{11}$$

By analogy with what was seen for Eq. (6), for the properties of the **R** matrix, Eq. (11) can be simplified as follows:

$$\begin{aligned} v_1 &= -2l_2r_{21}c_{\theta_2}l_1 - 2l_2r_{22}s_{\theta_2}l_1 - 2t_yl_1, \\ v_2 &= -2l_2r_{12}s_{\theta_2}l_1 - 2l_2r_{11}c_{\theta_2}l_1 - 2t_xl_1, \\ v_3 &= 2l_2\left(r_{11}t_x + r_{21}t_y + r_{31}t_z\right)c_{\theta_2} + \\ &\quad +2l_2\left(r_{12}t_x + r_{22}t_y + r_{32}t_z\right)s_{\theta_2} + t_x^2 + t_y^2 + t_z^2 + \\ &\quad +l_1^2 + l_2^2 - l_3^2 \end{aligned} \tag{12}$$

Eq. (10) is formally identical to Eq. (8), and this is due to the symmetry of the mechanism. The two solutions for $\theta_1$ are:

$$\begin{aligned} &\theta_{1A}, \theta_{1B} = \\ &atan2((v_2(v_3v_2 \pm V_1)/V_2 - v_3)/v_1, -(v_3v_2 \pm V_1)/V_2), \\ &V_1 = \sqrt{v_2^2v_1^2 + v_1^4 - v_1^2v_3^2}, \\ &V_2 = v_2^2 + v_1^2 \end{aligned} \tag{13}$$

*2.2.4. Ranges of rotations for the $\theta_1$ and $\theta_2$ angles*

Depending on the dimensions of the links, which are known, and the chosen pose of the movable frame, which must be measured, one, both, or none of the revolute joints $\mathbf{R}_1$ and $\mathbf{R}_2$ can perform a complete rotation. This means that the four-bar linkage is a double rocker, crank rocker, or double crank mechanism. Many researchers have proposed different methods to determine the mobility of a spatial $RSSR$ mechanism [43,44,47,48,53]. The classification can be determined by the intersection of the surfaces generated by the joints of the mechanism or by the sign of the radicands $K_1$ and $V_1$ of the Eqs. (9) and (13).

In the first approach, when one of the two ball joints (e.g. $S_2$) is disconnected, the mechanism is divided into a $RS$ arm with two links ($l_1$ and $l_2$) and a single link ($l_3$) with a $R$ joint. The working volume of the $RS$-arm is a torus, while the endpoint of the second arm describes a circle (Fig. 4, left). The intersection of the two working volumes defines the permissible configurations of the four-bar linkage. Four cases can occur:

- the circle is completely enclosed in the torus: the link $l_3$ is a crank (it can realize a complete rotation);
- an arc of the circle lies within the torus: the link $l_3$ is a rocker;
- two separate arcs of the circle lie within the torus: $l_3$ is a rocker and two different configurations are possible;
- the circle has no intersection with the torus: no configuration is allowed for the mechanism.

The procedure must be repeated, with the other spherical joint disconnected, to determine the mobility of the limb $l_1$ (Fig. 4, right). The problem of the intersection of a torus with a circle can be solved in closed form, so that the case encountered and the limits of the rotations can be easily determined.

The same results are obtained by numerically evaluating the radicands $K_1(\theta_1)$ and $V_1(\theta_2)$. The values of $\theta_1$ ($\theta_2$) that make $K_1$ ($V_1$) positive are the allowed angles of the $R_1$ ($R_2$) connection and the limits can be determined under the assumptions $K_1 = 0$ ($V_1 = 0$).

The permitted angle pairs $\theta_1$ and $\theta_2$ can be displayed in a Cartesian plane for a given pose. Since the angles are cyclic quantities, but the Cartesian dimensions are not, the solution locus can be better represented on the surface of a torus ($\theta_1$ is the angle of rotation, $\theta_2$ is the angle of the cross-section of the circle). Using these two representations, Figs. 5 and 6 show the most important possible mobility cases.

*2.2.5. Pose estimation procedure*

The actual end-effector pose, to be estimated, is the relative pose of the frame {2} with respect to the fixed frame {1}. For a $RSSR$ mechanism, with fixed geometric dimensions ($l_1$, $l_2$ and $l_3$ are known), it is represented by the rotation-translation matrix $\mathbf{M}_a$ (Eq. (14)), and can be described by a set of six coordinates $\mathbf{s}_a = [x_a\ y_a\ z_a\ \alpha_a\ \beta_a\ \gamma_a]^t$:

$$\begin{aligned} &\mathbf{M}_a(\mathbf{s}_a) = \\ &Tra(X, x_a) \cdot Tra(Y, y_a) \cdot Tra(Z, z_a) \cdot Rot(X, \alpha_a) \cdot \\ &\cdot Rot(Y, \beta_a) \cdot Rot(Z, \gamma_a) \end{aligned} \tag{14}$$

$N$ pairs of values of $\theta_1^i$ and $\theta_2^i$ ($\mathbf{\Theta}_m$) can be obtained by moving the two $R$ joints within the permissible ranges by simultaneous acquisition of the two encoders.

$$\mathbf{\Theta}_m = \begin{bmatrix} \theta_1^1 & \theta_2^1 \\ \theta_1^2 & \theta_2^2 \\ \vdots & \vdots \\ \theta_1^N & \theta_2^N \end{bmatrix}$$

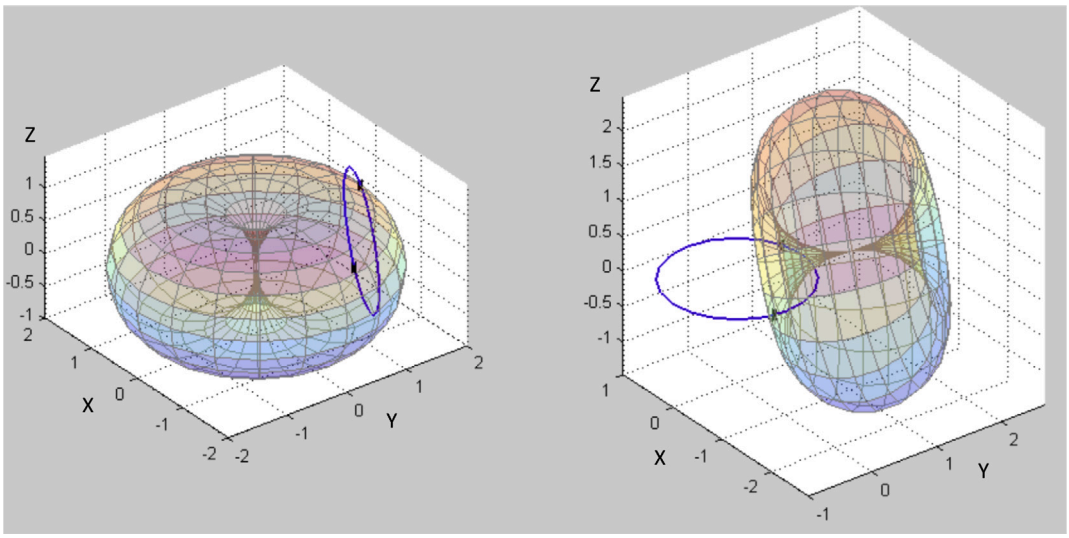


**Fig. 4.** Intersection of the working volume of the RS arm (torus) with those of the R link (circle).

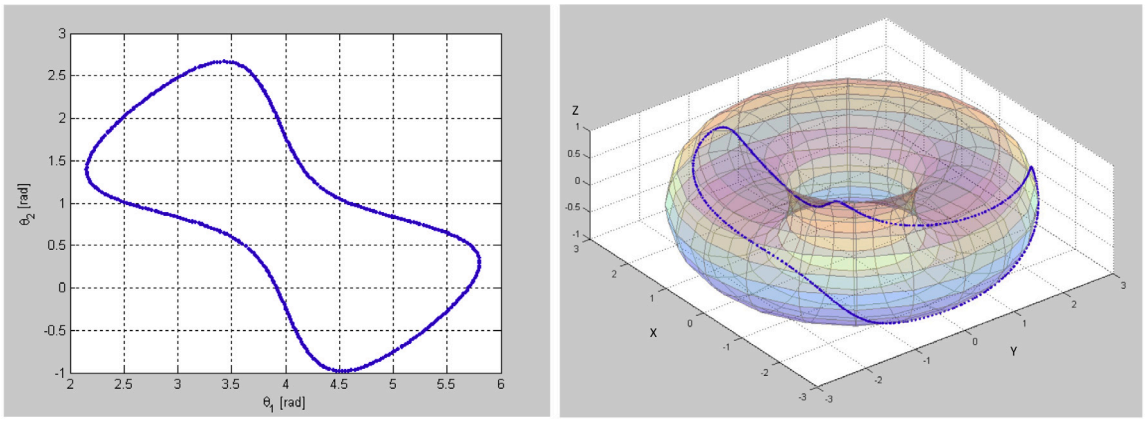


((a)) Double rocker with one allowable configuration.

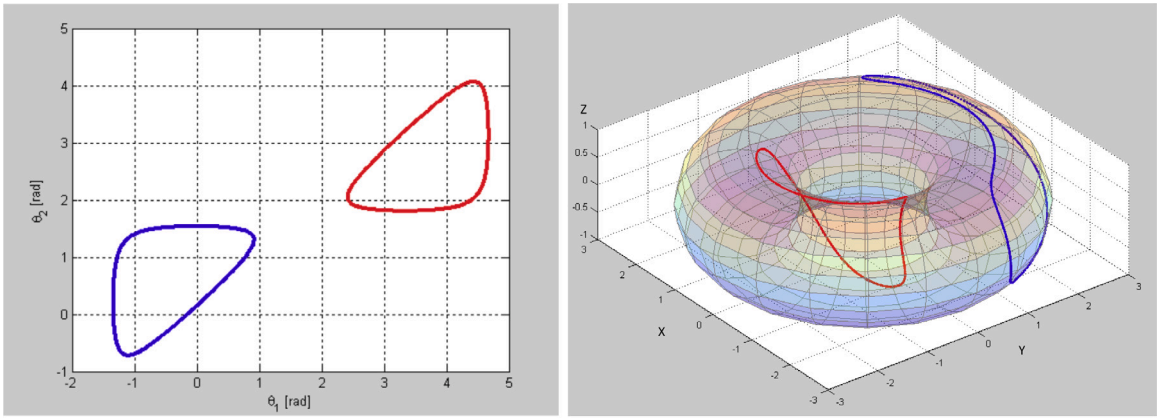


((b)) Double rocker with two allowable configurations.

**Fig. 5.** Graphs of the solution loci of $\theta_1$ and $\theta_2$ for the most important possible mobility cases - Part 1.

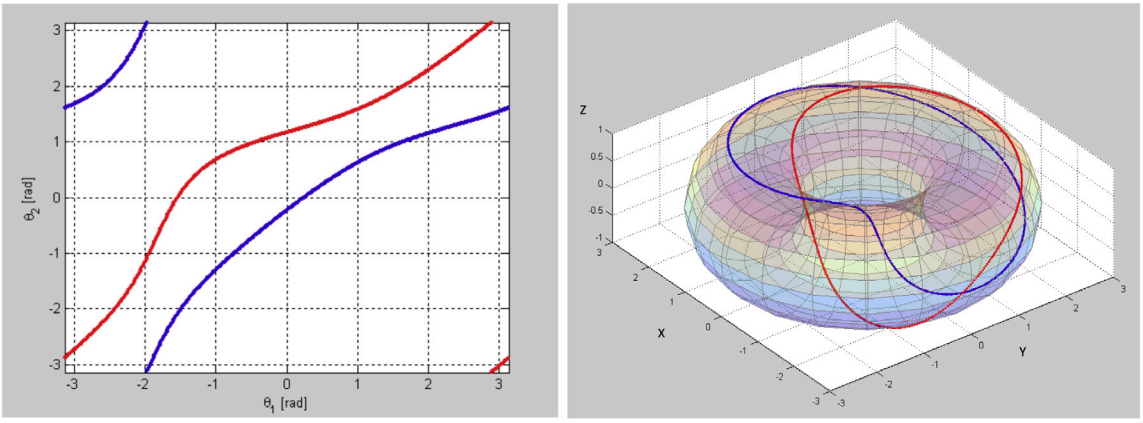


((a)) Double crank with two allowable configurations.

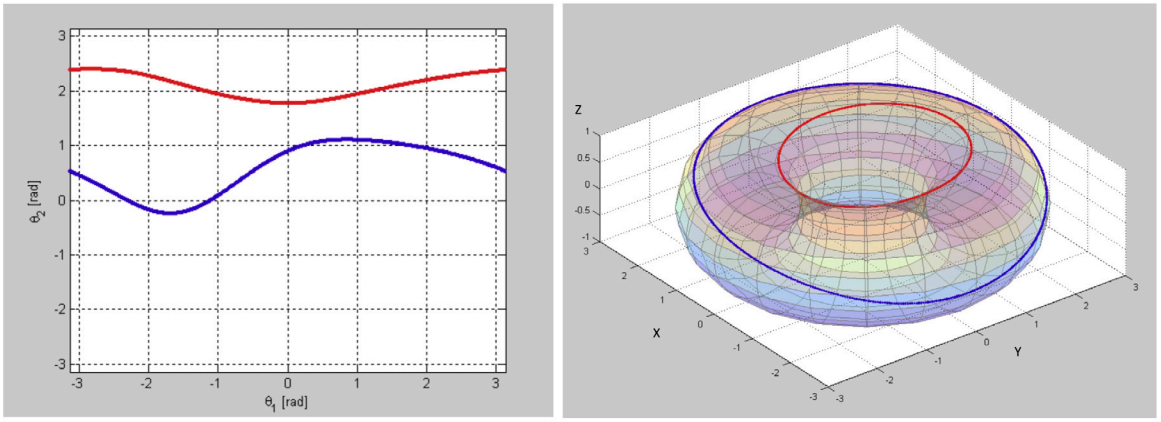


((b)) Crank-rocker with two allowable configurations.

**Fig. 6.** Graphs of the solution loci of $\theta_1$ and $\theta_2$ for the most important possible mobility cases - Part 2.

Since each pair of measured angles must satisfy the constraint equation Eq. (3), a system of $N$ equations can be written in the form of Eq. (15), where the six coordinates of $\mathbf{s}$ are the unknowns that must be determined by numerical algorithms.

$$f^i(\mathbf{M}(\mathbf{s}), \theta_1^i, \theta_2^i) = 0 \qquad i = 1 \dots N \tag{15}$$

In the general case, n = 6 independent configurations are sufficient. For n > 6 configurations (equations) the system is over constraint and the solution must be determined using least squares algorithms. In this case, the solution is more accurate and more robust against measurement errors due to the limited resolution or repeatability of the angle transducers used.

For a given estimate of the pose $\mathbf{s}_e$, the error vector $\mathbf{e}$ in the closure equations is expressed by Eq. (16).

$$\mathbf{e} = F\left(\mathbf{M}\left(\mathbf{s}_e\right), \mathbf{\Theta}_m\right) = \begin{bmatrix} f(\mathbf{M}(\mathbf{s_e}), \theta_1^1, \theta_2^1) \\ f(\mathbf{M}(\mathbf{s_e}), \theta_1^2, \theta_2^2) \\ \vdots \\ f(\mathbf{M}(\mathbf{s_e}), \theta_1^N, \theta_2^N) \end{bmatrix} \tag{16}$$

A better estimate for the current pose $\mathbf{s}_a$ can be calculated iteratively using the Newton–Raphson algorithm. The problem of finding the initial guess for initializing the Newton–Raphson method is easy to solve since calibration is usually done by moving the robot into a series of predefined poses (commanded poses). The measurement system is then used to measure the actual achieved pose (reaction poses), which is slightly different. Thus, for each pose, the known commanded pose is used to initialize the iterative procedure that determines the response pose. By adding the estimated pose $\mathbf{s}_{e,j}$ and the error $\mathbf{e}_j$ in the $j$th execution step, the numerical law is obtained, as expressed in Eq. (17), where $\mathbf{J}_{e,j}$ is a $(N \times 6)$ matrix and the operation $(\cdot)^+$ is the pseudo-inverse (required since $N > 6$).

$$\begin{cases} \mathbf{e}_j = F\left(\mathbf{M}\left(\mathbf{s}_{e,j}\right), \mathbf{\Theta}_m\right) \\ \mathbf{J}_{e,j} = \dfrac{\partial \mathbf{e}_j}{\partial \mathbf{s}_{e,j}} \end{cases} \quad \begin{cases} \mathbf{s}_{e,0} = \mathbf{s}_e \\ \mathbf{s}_{e,j+1} = \mathbf{s}_{e,j} - \mathbf{J}_{e,j}^+ \cdot \mathbf{e}_j \end{cases} \tag{17}$$

If the first trial solution $\mathbf{s}_{e,0}$ is sufficiently close to the actual pose $\mathbf{s}_a$, the iterations bring $\|\mathbf{e}_j\| \to 0$ and $\mathbf{s}_{e,j} \to \mathbf{s}_a$. The exact convergence of the algorithm can be hindered by several factors.

Every angle transducer (used to measure $\theta_1$ and $\theta_2$ angles) has an error due to limited accuracy, repeatability, and resolution. The (small) errors in measuring the angles prevent the closure equation from being satisfied when $N > 6$.

In addition, these errors cause uncertainties in the estimation $\mathbf{s}_e$ of the actual pose of the moving frame. The variance $\sigma^2_{tra}$ in the pose estimation $\left(\mathbf{s}_{e,tra} = [x_e \ y_e \ z_e]\right)$ is proportional to the dimension of the mechanism ($l_1$, $l_2$ and $l_3$), while the variance $\sigma^2_{rot}$ for the orientation $\left(\mathbf{s}_{e,rot} = [\alpha_e \ \beta_e \ \gamma_e]\right)$ is independent from them. Both are proportional to the variance $\sigma^2_\theta$ of the angle transducers and decrease as the number of measured angles increases:

$$\sigma_{tra} = k_{tra}\frac{\sigma_\theta}{\sqrt{N}} \qquad \sigma_{rot} = k_{rot}\frac{\sigma_\theta}{\sqrt{N}} \tag{18}$$

The values of $k_{tra}$ and $k_{rot}$ depend on the pose $\mathbf{s}$ and on the proportions between the limbs.

The mechanical inaccuracies (backlash and deflection) have the same effect on the fulfillment of the closure equation and on the accuracy of the pose estimation. For this reason, special care was taken in the development of the prototype.

The procedure for estimating the pose can be summarized in the following steps:

1. sensor installation: one end of the linkage is attached to the gripper and the other to the ground (global frame of reference);
2. positioning: the gripper is brought into the position to be measured and the robot's actuators are locked;
3. data acquisition: the $R$ joints are moved over the permissible range and several pairs of rotation angles $\theta_1$ and $\theta_2$ are recorded simultaneously. It is easy to collect a large number of readings as it is possible to record the two angles synchronously during a slow movement of the mechanism. One of the two $R$ joints can be driven by standard electric motors (when using two motors, appropriate control strategies must be used as the two rotations are not independent).
4. data processing: the recorded pairs of values of $\theta_1$ and $\theta_2$ and the known dimensions of the mechanism are used to form the system of non-linear equations (Eq. (15)) which can be solved using numerical algorithms, using the nominal pose as the first attempt solution.

### 2.3. Uncertainty analysis

The uncertainty of a measurement is a function of the specific measurement procedure used to obtain the measurement result, regardless of whether it is a simple or a complex procedure. Analyzing the measurement uncertainty provides an estimate of the largest error that can reasonably be expected for that specific measurement process.

Every angle transducer (used to measure $\theta_1$ and $\theta_2$ angles) has an error due to its limited accuracy, repeatability, and resolution. These errors lead to uncertainties in estimating the true pose of the moving frame. In other words, the estimated pose matrix $\mathbf{T}_e$ deviates from the actual $\mathbf{T}_a$. Since the error in estimating the pose is small, Eq. (19) can be written, where $dx \ dy \ dz$ and $d\alpha \ d\beta \ d\gamma$ are the linear and angular error, respectively.

$$d\mathbf{T} = \mathbf{T}_a\mathbf{T}_e^{-1} \simeq \left[\begin{array}{ccc|c} 1 & -d\gamma & d\beta & dx \\ d\gamma & 1 & -d\alpha & dy \\ -d\beta & d\alpha & 1 & dz \\ \hline 0 & 0 & 0 & 1 \end{array}\right] \tag{19}$$

The relationship between the error of the angle measurement $\mathbf{d\theta}$ and the error of the pose estimate $d\mathbf{s}$ can be determined by differentiating the constraint Eq. (3), as given in Eq. (20),

$$\mathbf{J}_{fm}\,\mathbf{J}_{ms}\,d\mathbf{s} + \mathbf{J}_{f\theta}\,d\boldsymbol{\theta} = 0 \tag{20}$$

where

$$\begin{aligned}
&d\mathbf{s} = [dx \quad dy \quad dz \quad d\alpha \quad d\beta \quad d\gamma]^t, \\
&\mathbf{t} = \left[r_{11} \quad r_{21} \quad r_{31} \quad r_{12} \quad r_{22} \quad r_{32} \quad r_{13} \quad r_{23} \quad r_{33} \quad t_x \quad t_y \quad t_z\right]^t, \\
&\boldsymbol{\theta} = \left[\theta_1 \quad \theta_2\right]^t, \\
&\mathbf{J}_{fm} = \frac{\partial f}{\partial \mathbf{t}} = \Big[m_1 c_{\theta_2} l_2 \quad m_2 c_{\theta_2} l_2 \quad m_3 c_{\theta_2} l_2 \quad m_1 s_{\theta_2} l_2 \quad m_2 s_{\theta_2} l_2 \\
&\ m_3 s_{\theta_2} l_2 \quad 0 \quad 0 \quad 0 \quad m_1 \quad m_2 \quad m_3\Big], \\
&m_1 = 2((r_{11}c_{\theta_2} + r_{12}s_{\theta_2})l_2 + t_x - l_1 c_{\theta_1}), \\
&m_2 = 2((r_{21}c_{\theta_2} + r_{22}s_{\theta_2})l_2 + t_y - l_1 s_{\theta_1}), \\
&m_3 = 2((r_{31}c_{\theta_2} + r_{32}s_{\theta_2})l_2 + t_z)
\end{aligned}$$

$$\mathbf{J}_{ms} = \frac{\partial \mathbf{t}}{\partial \mathbf{s}} = \begin{bmatrix} 0 & 0 & 0 & 0 & -r_{13} & r_{12} \\ 0 & 0 & 0 & 0 & -r_{23} & r_{22} \\ 0 & 0 & 0 & 0 & -r_{33} & r_{32} \\ 0 & 0 & 0 & r_{13} & 0 & -r_{11} \\ 0 & 0 & 0 & r_{23} & 0 & -r_{21} \\ 0 & 0 & 0 & r_{33} & 0 & -r_{31} \\ 0 & 0 & 0 & -r_{12} & r_{11} & 0 \\ 0 & 0 & 0 & -r_{22} & r_{21} & 0 \\ 0 & 0 & 0 & -r_{32} & r_{31} & 0 \\ r_{11} & r_{12} & r_{13} & 0 & 0 & 0 \\ r_{21} & r_{22} & r_{23} & 0 & 0 & 0 \\ r_{31} & r_{32} & r_{33} & 0 & 0 & 0 \end{bmatrix}$$

$$\mathbf{J}_{f\theta} = \frac{\partial f}{\partial \theta} = \Big[ p_1 s_{\theta_1} l_1 - p_2 c_{\theta_1} l_1 \quad p_1 l_2(-r_{11} s_{\theta_2} + r_{12} c_{\theta_2}) + \\ + p_2 l_2(-r_{21} s_{\theta_2} + r_{22} c_{\theta_2}) + p_3 l_2(-r_{31} s_{\theta_2} + r_{32} c_{\theta_2}) \Big],$$

$$p_1 = 2((r_{11} c_{\theta_2} + r_{12} s_{\theta_2}) l_2 + t_x - l_1 c_{\theta_1}),$$

$$p_2 = 2((r_{21} c_{\theta_2} + r_{22} s_{\theta_2}) l_2 + t_y - l_1 s_{\theta_1}),$$

$$p_3 = 2((r_{31} c_{\theta_2} + r_{32} s_{\theta_2}) l_2 + t_z)$$

To avoid singularity problems, it was chosen to calculate the pose error $d\mathbf{s}$ as a deviation from the actual pose $\mathbf{T}_a$.

Assuming that the measurement error of the angles $\theta_1$ and $\theta_2$ can be modeled with a normal distribution due to the limited repeatability and resolution, the covariance matrix of the vector $\mathbf{d\theta}$ is $\mathbf{C}_\theta$ (Eq. (21)). Since the two measures are independent, they are statistically uncorrelated and the matrix $\mathbf{C}_\theta$ is diagonal.

$$\mathbf{C}_\theta = \begin{bmatrix} \sigma_\theta^2 & 0 \\ 0 & \sigma_\theta^2 \end{bmatrix} = \sigma_\theta^2 \, \mathbf{I}_2 \tag{21}$$

If the two transducers are identical (which is plausible since the mechanism is symmetric), then $\mathbf{C}_\theta$ can be expressed according to Eq. (21), where $\sigma_\theta^2$ is the variance of the angle measure and $\mathbf{I}_2$ is the identity matrix.

The variance of the term $b = \mathbf{J}_{f\theta}\mathbf{d\theta}$ (cf Eq. (20)) for the $i$th configuration is estimated as given in Eq. (22), where $\mathbf{J}_{f\theta,i}$ is the Jacobian matrix $\mathbf{J}_{f\theta}$, which is evaluated for $\theta_1 = \theta_{1,i}$ and $\theta_2 = \theta_{2,i}$.

$$\sigma_{b,i}^2 = \mathbf{J}_{f\theta,i} \, \mathbf{C}_\theta \, \mathbf{J}_{f\theta,i}^t \tag{22}$$

Since the measures obtained in $N$ different configurations of the mechanism are uncorrelated to each other, the covariance matrix of the vector $\mathbf{b}_{tot} = [b_1 \; b_2 \; \dots \; b_n]^t$ is also diagonal:

$$\mathbf{C}_{b,tot} = diag(\sigma_{b,1}^2, \; \sigma_{b,2}^2, \; \dots, \; \sigma_{b,n}^2) \tag{23}$$

Considering Eq. (21), the covariance matrix of the vector $\mathbf{b}_{tot}$ can be reorganized as follows:

$$\mathbf{C}_{b,tot} = \sigma_\theta^2 \, \mathbf{C}_{f\theta} \tag{24}$$

where

$$\mathbf{C}_{f\theta} = \sigma_\theta^2 \; diag(\mathbf{J}_{f\theta,1}\mathbf{J}_{f\theta,1}^t, \; \mathbf{J}_{f\theta,2}\mathbf{J}_{f\theta,2}^t, \; \dots, \; \mathbf{J}_{f\theta,n}\mathbf{J}_{f\theta,n}^t)$$

Eq. (20) yields the covariance matrix $\mathbf{C}_s$ of the pose estimation error $d\mathbf{s}$ according to Eq. (25):

$$\mathbf{C}_s = \mathbf{J}_{fs,tot}^{+} \, \mathbf{C}_{b,tot} \, \mathbf{J}_{fs,tot}^{+t} = \sigma_\theta^2 \mathbf{J}_{fs,tot}^{+} \, \mathbf{C}_{f\theta} \, \mathbf{J}_{fs,tot}^{+t} \tag{25}$$

where

$$\mathbf{J}_{fs,tot} = \begin{bmatrix} \mathbf{J}_{fm,1}\mathbf{J}_{ms,1} \\ \mathbf{J}_{fm,2}\mathbf{J}_{ms,2} \\ \vdots \\ \mathbf{J}_{fm,n}\mathbf{J}_{ms,n} \end{bmatrix}$$

and $(\cdot)^+$ is the pseudo-inverse of a matrix.

The matrix $\mathbf{C}_s$ has the following form and is proportional to $\sigma_\theta^2$

$$\mathbf{C}_s = \left[\begin{array}{ccc|ccc} \sigma_x^2 & \sigma_{xy} & \sigma_{xz} & \sigma_{x\alpha} & \sigma_{x\beta} & \sigma_{x\gamma} \\ \sigma_{xy} & \sigma_y^2 & \sigma_{yz} & \sigma_{y\alpha} & \sigma_{y\beta} & \sigma_{y\gamma} \\ \sigma_{xz} & \sigma_{yz} & \sigma_z^2 & \sigma_{z\alpha} & \sigma_{z\beta} & \sigma_{x\gamma} \\ \hline \sigma_{x\alpha} & \sigma_{y\alpha} & \sigma_{z\alpha} & \sigma_\alpha^2 & \sigma_{\alpha\beta} & \sigma_{\alpha\gamma} \\ \sigma_{x\beta} & \sigma_{y\beta} & \sigma_{z\beta} & \sigma_{\alpha\beta} & \sigma_\beta^2 & \sigma_{\beta\gamma} \\ \sigma_{x\gamma} & \sigma_{y\gamma} & \sigma_{z\gamma} & \sigma_{\alpha\gamma} & \sigma_{\beta\gamma} & \sigma_\gamma^2 \end{array}\right] \tag{26}$$

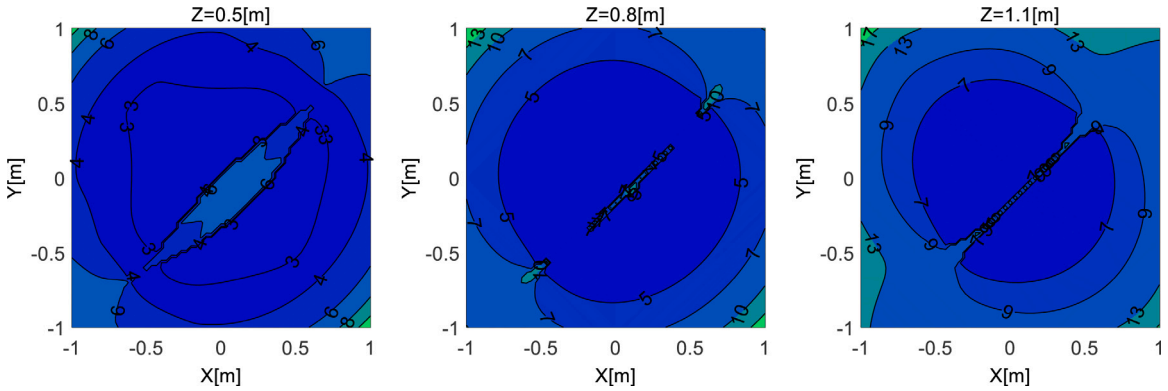


**Fig. 7.** Contour plot of the $k_{tra}$ index for three levels of the workspace.

$$\mathbf{C}_s = \sigma_\theta^2 \left[\begin{array}{c|c} \mathbf{C}_{tra} & \mathbf{C}_{tra-rot} \\ \hline \mathbf{C}_{tra-rot} & \mathbf{C}_{rot} \end{array}\right] = \sigma_\theta^2\, \mathbf{C}_{pos} \tag{27}$$

Depending on the application of the pose measurement method, it may be important to separately estimate the expected error in estimating the translation, rotation, or overall pose of the moving frame, as follows:

$$\begin{aligned} e_{tra} &= \sqrt{dx^2 + dy^2 + dz^2} \\ e_{rot} &= \sqrt{d\alpha^2 + d\beta^2 + d\gamma^2} \\ e_{pos} &= \sqrt{dx^2 + dy^2 + dz^2 + u^2(d\alpha^2 + d\beta^2 + d\gamma^2)} \end{aligned} \tag{28}$$

where $u$ is a constant used to compare rotational and translational errors.

It is important to note that the position estimation error increases proportionally with the dimensions ($l_1$, $l_2$ and $l_3$) of the mechanism (at the same ratio), while the rotation estimation error is independent of the scale.

$\sigma_{tra}^2$, $\sigma_{rot}^2$, and $\sigma_{pos}^2$ can be estimated as follows:

$$\sigma_{tra}^2 = \sigma_\theta^2 \left\|\mathbf{C}_{tra}\right\| \quad \sigma_{rot}^2 = \sigma_\theta^2 \left\|\mathbf{C}_{rot}\right\| \quad \sigma_{pos}^2 = \sigma_\theta^2 \left\|\mathbf{C}_{pos}\right\| \tag{29}$$

where $\|\cdot\|$ is the norm of a matrix corresponding to the maximum singular value of a matrix.

If the number $N$ of angular measures used for pose estimation is sufficiently large and the chosen angles are well distributed over the allowed rotation range, the values of $\sigma_{tra}^2$, $\sigma_{rot}^2$, and $\sigma_{pos}^2$ are inversely proportional to the number of measures $N$ (Eq. (30)).

$$\sigma_{tra} = k_{tra}\frac{\sigma_\theta}{\sqrt{N}} \quad \sigma_{rot} = k_{rot}\frac{\sigma_\theta}{\sqrt{N}} \quad \sigma_{pos} = k_{pos}\frac{\sigma_\theta}{\sqrt{N}} \tag{30}$$

The constants $k_{tra}$, $k_{rot}$ and $k_{pos}$ are defined as

$$\begin{aligned} k_{tra} &= \lim_{N\to\infty} \sqrt{N\ \left\|\mathbf{C}_{tra}\right\|} \\ k_{rot} &= \lim_{N\to\infty} \sqrt{N\ \left\|\mathbf{C}_{rot}\right\|} \\ k_{pos} &= \lim_{N\to\infty} \sqrt{N\ \left\|\mathbf{C}_{pos}\right\|} \end{aligned} \tag{31}$$

These constants are independent of the number $N$ and the variance $\sigma_\theta^2$ of the measured values, but vary only as a function of the pose of the moving frame, so they can be used as indices of the mechanism's ability to estimate this pose.

As an example, Figs. 7–9 show the numerical results of a special case. The mechanism has the dimensions $l_1 = l_2 = l_3 = 1$ [m]. The orientation of the movable frame is fixed and its position is moved over a three-dimensional grid:

$$\begin{aligned} &\mathbf{M} = Rot(X, 80)Rot(Y, 45)Tra(X, x_i)Tra(Y, y_i)Tra(Z, z_i) \\ &x_i = -1 \dots 1 \quad y_i = -1 \dots 1 \quad z_i = 0.5,\ 0.8,\ 1.1 \end{aligned} \tag{32}$$

with rotations expressed in degrees, and positions in meters.

It is noticeable that the values of all indices are quite small ($k_{tra} < 10$, $k_{rot} < 14$ and $k_{pos} < 18$) in almost all analyzed positions (a volume of $2 \times 2 \times 0.6$ [m]). This means that the uncertainty in estimating the pose is also low. Eq. (30) can be used to quickly determine the expected accuracy of the pose estimate. For digital encoders, the standard deviation $\sigma_\theta$ of the measure is related to the number of steps per revolution $n_{step}$ by the following relationship

$$\sigma_\theta = \frac{2\pi}{n_{step}\sqrt{12}} \simeq \frac{1.8}{n_{step}}\ [\text{rad}] \tag{33}$$

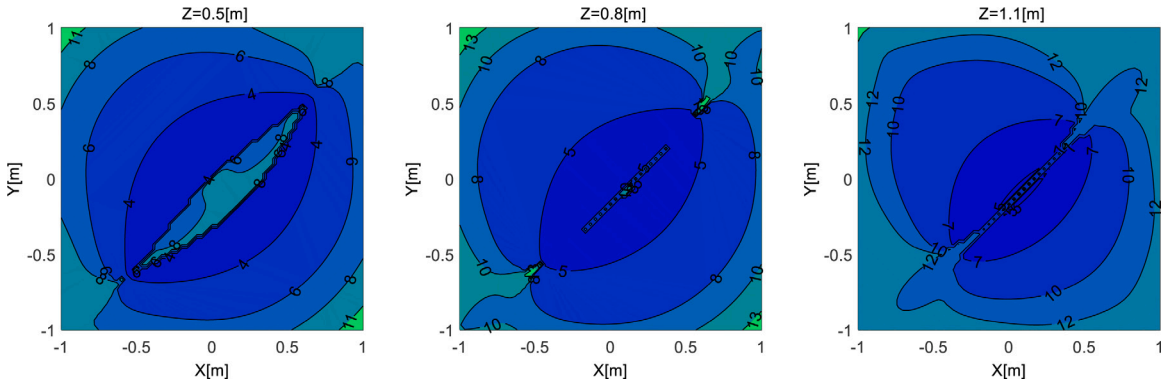


**Fig. 8.** Contour plot of the $k_{rot}$ index for three levels of the workspace.

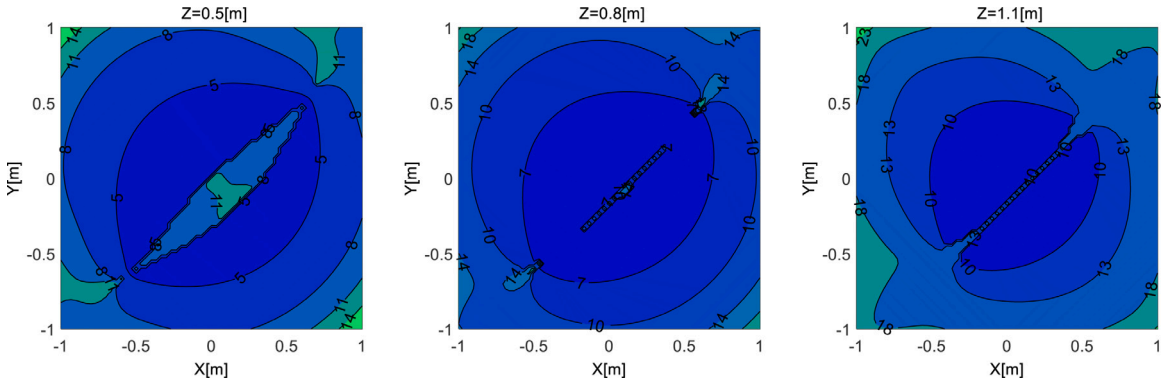


**Fig. 9.** Contour plot of the $k_{pos}$ index for three levels of the workspace.

By using two identical encoders with $n_{step} = 8000$ (2500 pulses per revolution), for the previous example, and by collecting $n = 2000$ pairs of measurements from $\theta_1$ and $\theta_2$ in each pose, Eq. (30) and (35) yield $\sigma_{theta} = 2.2 \cdot 10^{-4}$ [rad], $\sigma_{tra} = 5.1 \cdot 10^{-5}$ [m], $\sigma_{rot} = 7.1 \cdot 10^{-5}$ [rad] and using $u = 1$ [m/rad], $\sigma_{pos} = 9.1 \cdot 10^{-5}$ [m].

Since other sources of error may also be present (backlash, geometric inaccuracies, deflections), the estimation error for the position is expected to be less than 0.1 [mm] (much less than one ten-thousandth of the full scale) and for orientation less than 0.1 [mrad].

## 3. Experiments on a linkage-based measuring mechanism prototype

### 3.1. Description of the prototype of linkage-based measuring mechanism

Fig. 10 shows the created prototype of the proposed linkage-based measuring device. The aim of the realization of the prototype is the experimental validation of the measurement method and an initial assessment of the achievable repeatability and accuracy of the system.

In terms of mechanical design, the revolute joints are derived directly from the shafts of the encoders (with reinforced ball bearings), while the ball joints have been specially developed (Fig. 11). The correct operation of the measurement system is closely related to the angular mobility of the ball joints and the presence of low backlash and friction in the joints. All these objectives were achieved by realizing the joint with an iron ball held in contact with a conical seat (made of Teflon) by the attractive force of a magnet. This low-cost joint ensures a large angular movement (more than $2\pi$ [sr]), no backlash (thanks to the self-centering unilateral constraint), and low friction.

There is a certain freedom in the choice of geometric dimensions of the device. The main constraints to be considered concern the ratio between the lengths of the different links, on which important mechanical aspects such as the possible mechanical bending depend. The diameter of the rods also has a major influence on this aspect, as does the material chosen for their construction. In the prototype created, the geometric dimensions chosen, both in terms of the length of the links and the diameter of the rods, give the system considerable structural stability with very limited possible deformations. Given the small dimensions, no special analyses were carried out. The dimensions of the links determine the measuring range of the system. Larger dimensions are of course possible and can extend the measuring range considerably. In this case, a finite element analysis of the structure, simulating the possible

**Fig. 10.** The realized prototype of linkage-based measuring device.

**Fig. 11.** Close view of a spherical joint.

loading conditions and the most critical working configurations, can be important for an adequate dimensioning of the mechanical structure of the system.

To reduce deflection, the connections were made with lightweight aluminum tubes with a large cross-section. The entire structure is statically balanced with additional masses so that it can remain at rest in any position (indifferent equilibrium).

The angular position encoders of the revolute joints are two incremental encoders with 10,000 pulses/revolution ($n_{step} = 40000$ pulses/revolution according to hardware multiplier). Their synchronous acquisition is performed by an ISA DSP-based card with 1 kHz. The resolution of the encoder is evaluated as in Eq. (34).

$$\theta_{resolution} = \frac{2\pi}{n_{step}} = \frac{2\pi}{40000} = 1.57 \cdot 10^{-4} \text{ [rad]}; \tag{34}$$

The random error in Eq. (34) is uniformly distributed around zero because the encoders divide a full revolution into several predefined steps (in our case 40,000) and the sensor provides the same output for each angle in this interval. The reading error is therefore distributed around zero with the same probability in the $360°/n_{step}$ range.

Taking into account the uniform error distribution caused by the limited resolution, the standard deviation of the angular measure is given in (35).

$$\sigma_\theta = \frac{2\pi}{n_{step}\sqrt{12}} = 4.5 \cdot 10^{-5} \text{ [rad]} \tag{35}$$

### 3.2. Measure of the geometrical elements

The system was calibrated using a coordinate measuring machine (CMM) with a resolution of $1 \cdot 10^{-6}$ [m], a repeatability of $3 \cdot 10^{-6}$ [m] and an accuracy of $5 \cdot 10^{-6}$ [m].

First, the geometric dimensions of the prototype were measured: the length of the rod ($l_3$) was determined by measuring the distance between the centers of the spheres at its ends, while for the lengths of the cranks ($l_1$ and $l_2$) the axes of the encoder shafts and the center of each sphere were used.

**Table 2**
Geometrical dimensions of the elements of the prototype.

| | | Nominal dimensions [m] | Measured dimension [m] |
|---|---|---|---|
| Spheres diameters | $S_1$ | 0.0254 | 0.025405 |
| | $S_2$ | 0.0254 | 0.025409 |
| Cranks length | $l_1$ | 0.250 | 0.250825 |
| | $l_2$ | 0.250 | 0.250768 |
| Rod length | $l_3$ | 0.250 | 0.250358 |

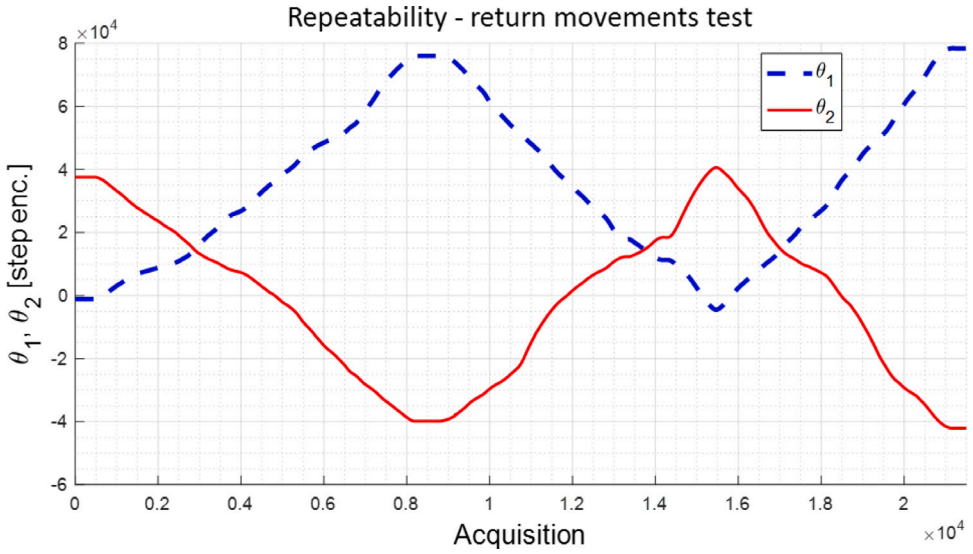


**Fig. 12.** Joint movements for the measure of the uncertainty of the pose estimation procedure.

The reverse engineering software of the CMM was used to identify the geometric objects (spheres and cylinders). The resolution of the dimensions of the geometric objects is $1 \cdot 10^{-6}$ [m] for the linear dimensions and $5 \cdot 10^{-4}$ [rad] for the angular dimensions (alignment of the cylinder axes). The limited resolution when measuring angles restricts the resolution of the software when measuring the relative position of objects. Namely, if $d \simeq 0.25$ [m] is used to specify the maximum dimension of the prototype to be measured, the CMM can measure the relative positions of objects with a resolution of $\simeq 5 \cdot 10^{-4} \cdot d = 1.25 \cdot 10^{-4}$ [m].

The geometrical dimensions of the prototype are reported in Table 2.

### 3.3. Uncertainty analysis of the pose estimation procedure

To measure the uncertainty of the pose estimation, several forward and backward movements of the **R** joints in different configurations were investigated (see e.g. Fig. 12). The pairs $(\theta_1^i, \theta_2^i)$ relating to the movement shown in Fig. 12 are represented in Fig. 13.

During the movement, pairs of values $(\theta_1^i, \theta_2^i)$ were recorded synchronously. Since it is very easy to collect many experimental points for each pose, two thousand values for each pose have been collected. Based on this data, the relative pose **M** was determined using the algorithm proposed in Section 2.2.5. Then, for each $\theta_1^i$ and $\theta_2^i$ the corresponding values of $\theta_{2,est}^i$ and $\theta_{1,est}^i$ were computed using the Eq. (13) and (9) respectively (see Fig. 14). The angular errors expressed in Eq. (36) are not suitable for the evaluation of repeatability, as their value depends strongly on the local slope of the solution loci (Fig. 6).

$$\Delta\theta_1^i = \theta_1^i - \theta_{1,est}^i \qquad \Delta\theta_2^i = \theta_2^i - \theta_{2,est}^i \tag{36}$$

A more effective measure of the angular error is given in (37).

$$\Delta\theta^i = \frac{\Delta\theta_1^i \, \Delta\theta_2^i}{\sqrt{\left(\Delta\theta_1^i\right)^2 + \left(\Delta\theta_2^i\right)^2}} \tag{37}$$

The standard deviation of $\Delta\theta^i$, given by $u(\Delta\theta)$, can be seen as a measure of the uncertainty of the system for the angular position. The difference between the standard deviation $\sigma_\theta$ determined for the encoders (Eq. (35)) and $u(\Delta\theta)$ can be used as a measure of the other sources of error that may be present, such as backlash, geometric inaccuracies, and deflections.

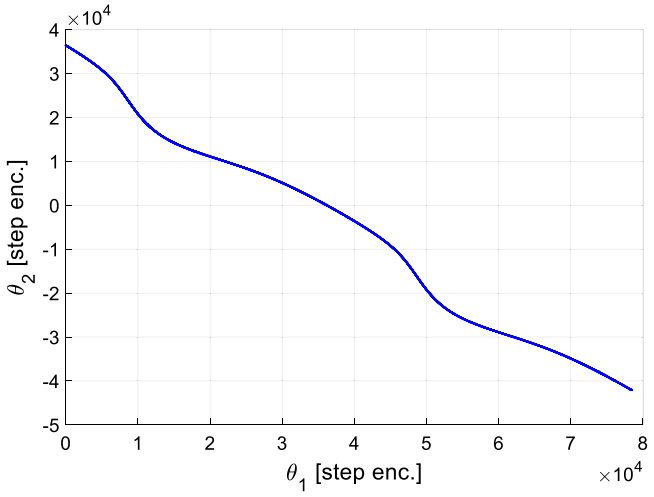


**Fig. 13.** Plot of the points $(\theta_1^i, \theta_2^i)$ of Fig. 12.

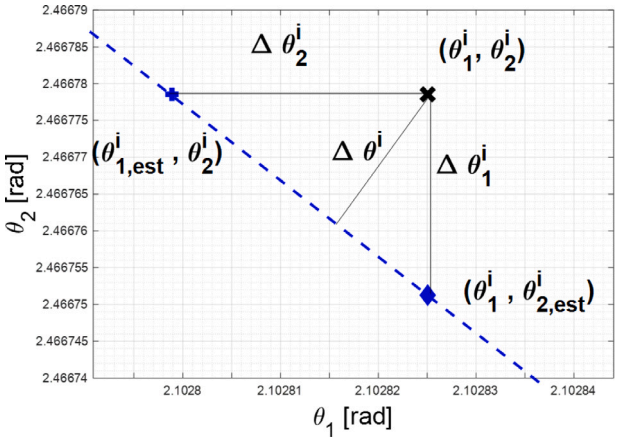


**Fig. 14.** Representation of $\Delta\theta_1^i$, $\Delta\theta_2^i$, $\Delta\theta^i$.

The relation between the error in the angle measurement $\Delta\theta$ and the error in the pose estimation $\Delta\mathbf{s}$ can be determined by differentiating the constraint equation Eq. (3):

$$\mathbf{J}_{fm}\,\mathbf{J}_{ms}\,d\mathbf{s} + \mathbf{J}_{f\theta}\,d\boldsymbol{\theta} = 0 \qquad \Delta\mathbf{s} \backsimeq -\mathbf{J}_{ms}^{-1}\,\mathbf{J}_{fm}^{-1}\,\mathbf{J}_{f\theta}\,\Delta\boldsymbol{\theta} \tag{38}$$

where

$$\begin{cases} d\mathbf{s} &= \begin{bmatrix} dx & dy & dz & d\alpha & d\beta & d\gamma \end{bmatrix}^t \\ \mathbf{m} &= \begin{bmatrix} m_1 & \dots & m_i & \dots & m_{12} \end{bmatrix}^t \\ \boldsymbol{\theta} &= \begin{bmatrix} \theta_1 & \theta_2 \end{bmatrix}^t \end{cases} \qquad \begin{cases} \mathbf{J}_{fm} = \partial f/\partial \mathbf{m} \\ \mathbf{J}_{ms} = \partial \mathbf{m}/\partial \mathbf{s} \\ \mathbf{J}_{f\theta} = \partial f/\partial \theta \end{cases} \tag{39}$$

$\mathbf{m}$ is the vector containing the first 12 elements of the matrix $\mathbf{M}$ and the matrices $\mathbf{J}_{fm}$, $\mathbf{J}_{ms}$ and $\mathbf{J}_{f\theta}$ are functions of $(\theta_1, \theta_2)$. Since $(\theta_1^i, \theta_2^i)$ cannot be a solution of the Eq. (3) due to measurement errors, $\left(\theta_1^i, \theta_{2,est}^i\right)$ and $\left(\theta_{1,est}^i, \theta_2^i\right)$ can be used correctly in their place. As in Eq. (30), the positional error $\Delta\mathbf{s}_{tra}^i$ can be separated from the angular error $\Delta\mathbf{s}_{red}^i$. The uncertainty $u\left(\Delta\mathbf{s}_{tra}\right)$ and $u\left(\Delta\mathbf{s}_{rot}\right)$ are calculated using the standard deviations.

Table 4 contains the experimental results for the 3 different poses of the Table 3. The small value of $u(\Delta\theta)$ shows the high repeatability of the system. As $u(\Delta\theta)$ is almost twice as high as the theoretical value $\sigma_\theta = 4.5{\cdot}10^{-5}$ [rad], the mechanical inaccuracy due to backlash and deflection is very small (its influence is almost as large as the error due to the encoder resolution), but cannot be neglected. In addition, the agreement between the theoretical values $\sigma_{tra}$ and $\sigma_{rot}$ is also quite good. A statistical determination of the uncertainty must be investigated over the entire working area.

**Table 3**
Measured poses.

| | | Pose 1 | Pose 2 | Pose 3 |
|---|---|---|---|---|
| $X$ | [m] | 0.044 | 0.069 | 0.043 |
| $Y$ | [m] | 0.108 | 0.143 | 0.143 |
| $Z$ | [m] | 0.147 | 0.150 | 0.055 |
| $\alpha$ | [rad] | −2.984 | 2.813 | −2.758 |
| $\beta$ | [rad] | 0.029 | 0.143 | −0.306 |
| $\gamma$ | [rad] | 0.250 | 0.255 | −1.118 |

**Table 4**
Values for standard deviation and uncertainty in the pose reported in Table 3.

| Theoretical results | | | | |
|---|---|---|---|---|
| | | Pose 1 | Pose 2 | Pose 3 |
| $k_{tra}$ | [-] | 26.4 | 4.0 | 34.3 |
| $k_{rot}$ | [-] | 119.8 | 18.8 | 58.1 |
| $\sigma_{tra}$ | [m] | $4.4 \cdot 10^{-5}$ | $1.1 \cdot 10^{-5}$ | $1.7 \cdot 10^{-5}$ |
| $\sigma_{rot}$ | [rad] | $1.0 \cdot 10^{-5}$ | $5.3 \cdot 10^{-5}$ | $2.9 \cdot 10^{-5}$ |
| **Experimental results** | | | | |
| | | Pose 1 | Pose 2 | Pose 3 |
| $max(\Delta\theta)$ | [rad] | $20.7 \cdot 10^{-5}$ | $63.5 \cdot 10^{-5}$ | $44.8 \cdot 10^{-5}$ |
| $u(\Delta\theta)$ | [rad] | $7.9 \cdot 10^{-5}$ | $8.5 \cdot 10^{-5}$ | $9.4 \cdot 10^{-5}$ |
| $u\left(\Delta\mathbf{s}_{tra}\right)$ | [m] | $13.6 \cdot 10^{-5}$ | $1.4 \cdot 10^{-5}$ | $0.6 \cdot 10^{-5}$ |
| $u\left(\Delta\mathbf{s}_{rot}\right)$ | [rad] | $0.9 \cdot 10^{-5}$ | $9.0 \cdot 10^{-5}$ | $2.8 \cdot 10^{-5}$ |

**Table 5**
Comparison between the pose measured by the CMM and the estimated one.

| | | Pose measured | Pose estimated | Pose error | | |
|---|---|---|---|---|---|---|
| $X$ | [m] | 0.044 292 | 0.044 199 | $dx$ | [m] | $8.7 \cdot 10^{-5}$ |
| $Y$ | [m] | 0.107 981 | 0.107 887 | $dy$ | [m] | $10.6 \cdot 10^{-5}$ |
| $Z$ | [m] | 0.147 886 | 0.147 655 | $dz$ | [m] | $5.8 \cdot 10^{-5}$ |
| $\alpha$ | [rad] | −2.9813 | −2.9831 | $d\alpha$ | [rad] | $1.7 \cdot 10^{-3}$ |
| $\theta$ | [rad] | 0.02874 | 0.0292 | $d\beta$ | [rad] | $0.4 \cdot 10^{-3}$ |
| $\gamma$ | [rad] | 0.24841 | 0.2488 | $d\gamma$ | [rad] | $0.5 \cdot 10^{-3}$ |

### 3.4. First calibration tests

The agreement between the actual position measured by the CMM (Section 3.2) and the estimated position was tested. The prototype was positioned in the working area of the CMM. The absolute position of the frame {1} attached to the first encoder and the frame {2} attached to the second encoder was measured by estimating the position of the shaft axes of the encoder and the ball centers of the ball joints.

Given $\mathbf{M}_a$ and $\mathbf{M}_e$ as the rotation-translation matrix describing the actual position measured by the CMM and the estimated position, respectively, the error in pose estimation is calculated according to Eq. (40).

$$\Delta\mathbf{M} = \mathbf{M}_a\mathbf{M}_e^{-1} \simeq \left[\begin{array}{ccc|c} 1 & -d\gamma & d\beta & dx \\ d\gamma & 1 & -d\alpha & \\ -d\beta & d\alpha & 1 & \\ \hline 0 & 0 & 0 & 1 \end{array}\right] \tag{40}$$

$dx$, $dy$, $dz$, and $d\alpha$, $d\beta$, $d\gamma$ are the linear and angular errors respectively.

Table 5 shows the estimated pose error for an exemplary experiment. The third column indicates the value for the error represented by Eq. (40). It can be seen that both the linear and angular errors are close to the resolution provided by the processing software of the CMM (see Section 3.2). This preliminary result provides proof of the correctness of the measurement system and a first estimate of the achievable accuracy.

## 4. Conclusions

A new method for pose measurement is proposed based on the measurement of joint rotation of a spatial four-bar mechanism. The method for estimating both the position coordinates and the uncertainty has been developed in analytical form. The main advantages of the proposed method are:

– all six coordinates of the pose moving frame can be measured simultaneously;

- for a given pose to be measured, a large number of measurements of the rotation of the **R** joints can be easily collected. This property of the method can greatly reduce the uncertainty of the estimate;
- the kinematic structure of the mechanism is simple ($RSSR$), therefore it can be easily realized with high accuracy (low backlash and low deformations);
- the measuring range of the mechanism is quite large (e.g. a mechanism with $l_1 = l_2 = l_3 = l$ can measure a volume of $2l \times 2l \times l$, depending on the position of the moving frame);
- the required sensors (two digital encoders are suitable) are simple, generally usable, and therefore cheap.

There are also some disadvantages:

- measuring the pose requires the contact with the body to be measured;
- the procedure appears to apply only to static measures;
- deformations and backlashes in the mechanical structure of the four-bar linkage cause measurement errors (not investigated in this work);
- within the achievable measurement volume of the mechanism, some singular configurations may occur that lead to a high uncertainty in the estimation of one or more of the position coordinates. These poses can be detected by examination if $rank(J_{fs,tot}) < 6$ and have a correspondence in high values of the indices $k_{tra}$, $k_{rot}$ and $k_{pos}$. A singular configuration exists, for example, if $l_1 = l_2$, the axes $z_1$ and $z_2$ coincide and the distance between the frames is equal to $l_3$ (the rotation around $z_2$ is indeterminable). These configurations must be avoided or the singularity can be eliminated by repositioning the mobile or the reference frame.

The following issues stem from comparing the proposed system with other strategies suggested in the literature or often utilized in practical applications. The double ball bar system, inclinometer, interferometers, and laser tracker techniques can only measure a portion of the pose coordinates, while the suggested solution enables a full position measurement. The primary drawback, as compared to laser tracking systems, is the lower accuracy. Conversely, the system is more cost-effective since it utilizes two standard digital encoders and straightforward ball joint construction. The primary benefit of this approach over others based on dimes is the potential for a broader range of measurement. The measuring is easier compared to camera-based alternatives. However, these approaches do not need interaction with the end effector. The precision achieved is markedly higher when compared to approaches utilizing wires.

The experiments only served to test the feasibility of the measurement system and an initial assessment of its accuracy.

The experimental results show that the measuring system has an accuracy of about $1{\cdot}10^{-5}$ [m] when estimating the linear position of an object in space and about $1{\cdot}10^{-4}$ [rad] when estimating the angular position.

This accuracy result may be sufficient for some types of robotic applications, such as palletizing, painting, surface treatment, etc. For applications requiring better position and/or orientation accuracy, the developed device prototype would not be suitable. However, the proposed approach is also valid for these applications and a design solution of the device with improved constructive characteristics can certainly lead to an improvement of both position and orientation accuracy. The main objectives of this work were to propose a methodology, to show that it is promising, and that even with a first prototype acceptable results in terms of accuracy have been obtained for some types of applications. However, there is still plenty of scope for improving the achievable measurement accuracy.

Future work is planned in this direction to develop a constructive implementation of the device that will improve its accuracy.

A statistical determination of the accuracy and repeatability of the system has not been developed and will be the subject of future work.

The natural development of the work will also concern the application of the proposed method to the calibration of an industrial robot, comparing the results obtained when measuring the pose with laser trackers or other methods.

## CRediT authorship contribution statement

**Monica Tiboni:** Writing – review & editing, Writing – original draft, Supervision, Methodology, Formal analysis, Data curation, Conceptualization, Software. **Giovanni Legnani:** Funding acquisition, Conceptualization, Methodology, Supervision, Writing – review & editing. **Roberto Bussola:** Data curation, Software, Validation, Writing – review & editing. **Diego Tosi:** Conceptualization, Data curation, Methodology, Validation, Writing – original draft.

## Declaration of competing interest

The authors declare that they have no known competing financial interests or personal relationships that could have appeared to influence the work reported in this paper.

## Data availability

The authors do not have permission to share data.

## References


[1] Z. Roth, B. Mooring, B. Ravani, An overview of robot calibration, IEEE J. Robot. Autom. 3 (5) (1987) 377–385, http://dx.doi.org/10.1109/JRA.1987.1087124.

[2] J. Chen, L.-M. Chao, Positioning error analysis for robot manipulators with all rotary joints, IEEE J. Robot. Autom. 3 (6) (1987) 539–545, http://dx.doi.org/10.1109/JRA.1987.1087144.

[3] M.R. Driels, W.E. Swayze, Automated partial pose measurement system for manipulator calibration experiments, IEEE Trans. Robot. Autom. 10 (4) (1994) 430–440.

[4] D.E. Whitney, C.A. Lozinski, J.M. Rourke, Industrial robot forward calibration method and results, J. Dyn. Syst. Meas. Control 108 (1) (1986) 1–8, http://dx.doi.org/10.1115/1.3143737.

[5] J. Jarvis, Microsurveying: Towards robot accuracy, in: Proceedings. 1987 IEEE International Conference on Robotics and Automation, Vol. 4, 1987, pp. 1660–1665, http://dx.doi.org/10.1109/ROBOT.1987.1087739.

[6] Y. Wu, A. Klimchik, S. Caro, B. Furet, A. Pashkevich, Geometric calibration of industrial robots using enhanced partial pose measurements and design of experiments, Robot. Comput.-Integr. Manuf. 35 (2015) 151–168, http://dx.doi.org/10.1016/j.rcim.2015.03.007.

[7] K.L. Conrad, T.C. Yih, Robotic calibration issues: Accuracy, repeatability and calibration, in: 8th Mediterranean Conference on Control & Automation, No. July, 2000, pp. 17–19.

[8] X.-L. Zhong, J. Lewis, A new method for autonomous robot calibration, in: Proceedings of 1995 IEEE International Conference on Robotics and Automation, Vol. 2, 1995, pp. 1790–1795 vol.2, http://dx.doi.org/10.1109/ROBOT.1995.525529.

[9] K.C. P.S. Shiakolas, T. Yih, On the accuracy, repeatability, and degree of influence of kinematics parameters for industrial robots, Int. J. Modelling Simul. 22 (4) (2002) 245–254, http://dx.doi.org/10.1080/02286203.2002.11442246.

[10] Chen-Gang, Li-Tong, Chu-Ming, J.Q. Xuan, S.H. Xu, Review on kinematics calibration technology of serial robots, Int. J. Precis. Eng. Manuf. 15 (8) (2014) 1759–1774, http://dx.doi.org/10.1007/s12541-014-0528-1.

[11] L. Miao, Y. Zhang, Z. Song, Y. Guo, W. Zhu, Y. Ke, A two-step method for kinematic parameters calibration based on complete pose measurement—Verification on a heavy-duty robot, Robot. Comput.-Integr. Manuf. 83 (2023) 102550, http://dx.doi.org/10.1016/j.rcim.2023.102550.

[12] Y. Lingtao, W. Jian, D. Zhijiang, S. Lining, C. Hegao, A novel method on parallel robot's pose measuring and calibration, in: 2007 2nd IEEE Conference on Industrial Electronics and Applications, 2007, pp. 1292–1296, http://dx.doi.org/10.1109/ICIEA.2007.4318614.

[13] R. He, Y. Zhao, S. Yang, S. Yang, Kinematic-parameter identification for serial-robot calibration based on POE formula, IEEE Trans. Robot. 26 (3) (2010) 411–423, http://dx.doi.org/10.1109/TRO.2010.2047529.

[14] G. Chen, H. Wang, Z. Lin, Determination of the identifiable parameters in robot calibration based on the POE formula, IEEE Trans. Robot. 30 (5) (2014) 1066–1077, http://dx.doi.org/10.1109/TRO.2014.2319560.

[15] X. Chen, Q. Zhan, The kinematic calibration of an industrial robot with an improved beetle swarm optimization algorithm, IEEE Robot. Autom. Lett. 7 (2) (2022) 4694–4701.

[16] G. Luo, L. Zou, Z. Wang, C. Lv, J. Ou, Y. Huang, A novel kinematic parameters calibration method for industrial robot based on levenberg-marquardt and differential evolution hybrid algorithm, Robot. Comput.-Integr. Manuf. 71 (2021) 102165, http://dx.doi.org/10.1016/j.rcim.2021.102165.

[17] E. Nieves, N. Xi, X. Li, C. Martinez, G. Zhang, Laser beam multi-position alignment approach for an automated industrial robot calibration, in: 4th Annual IEEE International Conference on Cyber Technology in Automation, Control and Intelligent Systems, IEEE-CYBER 2014, IEEE, 2014, pp. 359–364, http://dx.doi.org/10.1109/CYBER.2014.6917490.

[18] A. Nubiola, I.A. Bonev, Absolute calibration of an ABB IRB 1600 robot using a laser tracker, Robot. Comput.-Integr. Manuf. 29 (1) (2013) 236–245, http://dx.doi.org/10.1016/j.rcim.2012.06.004.

[19] G.-r. Tang, L.-s. Liu, Robot calibration using a single laser displacement meter, Mechatronics 3 (4) (1993) 503–516, http://dx.doi.org/10.1016/0957-4158(93)90020-3.

[20] M.R. Driels, W. Swayze, S. Potter, Full-pose calibration of a robot manipulator using a coordinate-measuring machine, Int. J. Adv. Manuf. Technol. 8 (1) (1993) 34–41, http://dx.doi.org/10.1007/BF01756635.

[21] J.-H. Borm, C.-H. Meng, Determination of optimal measurement configurations for robot calibration based on observability measure, Int. J. Robot. Res. 10 (1) (1991) 51–63, http://dx.doi.org/10.1177/027836499101000106.

[22] T.J. Legnani G., Mina C., Static calibration of industrial manipulators: Design of an optical instrumentation and application to SCARA robots, J. Robot. Syst. 13 (7) (1996) 445–460.

[23] A. Omodei, G. Legnani, R. Adamini, Three methodologies for the calibration of industrial manipulators: Experimental results on a SCARA robot, J. Robot. Syst. 17 (6) (2000) 291–307.

[24] Y. Bai, H. Zhuang, Z.S. Roth, Experiment study of PUMA robot calibration using a laser tracking system, in: SMCia 2003 - Proceedings of the 2003 IEEE International Workshop on Soft Computing in Industrial Applications, 2003, pp. 139–144, http://dx.doi.org/10.1109/SMCIA.2003.1231359.

[25] G.D. van Albada, J.M. Lagerberg, A. Visser, L.O. Hertzberger, A low-cost pose-measuring system for robot calibration, Robot. Auton. Syst. 15 (3) (1995) 207–227, http://dx.doi.org/10.1016/0921-8890(95)00038-H.

[26] R.A. Boby, Kinematic identification of industrial robot using end-effector mounted monocular camera bypassing measurement of 3-D pose, IEEE/ASME Trans. Mechatronics 27 (1) (2022) 383–394, http://dx.doi.org/10.1109/TMECH.2021.3064916.

[27] A. Rauf, A. Pervez, J. Ryu, Experimental results on kinematic calibration of parallel manipulators using a partial pose measurement device, IEEE Trans. Robot. 22 (2) (2006) 379–384, http://dx.doi.org/10.1109/TRO.2006.862493.

[28] A.P. Robertson, P.J. Willoughby, A. Slocum, Precision robot calibration using kinematically placed inclinometers, in: ASPE Proceedings, 2001, pp. 2–5.

[29] G. Canepa, J.M. Hollerbach, A.J. Boelen, Kinematic calibration by means of a triaxial accelerometer, in: Proceedings - IEEE International Conference on Robotics and Automation, (pt 4) 1994, pp. 2776–2782, http://dx.doi.org/10.1109/robot.1994.350917.

[30] P.U.S. Driels M. R., Vision-based automatic theodolite for robot calibration, IEEE Trans. Robot. Autom. 7 (3) (1991) 351–360.

[31] M. Driels, U. Pathre, Robot calibration using an automatic theodolite, Int. J. Adv. Manuf. Technol. 9 (2) (1994) 114–125, http://dx.doi.org/10.1007/BF01750418.

[32] H. Zhuang, O. Masory, J. Yan, Kinematic calibration of a Stewart platform using pose measurements obtained by a single theodolite, in: IEEE International Conference on Intelligent Robots and Systems, Vol. 2, 1995, pp. 329–334, http://dx.doi.org/10.1109/iros.1995.526237.

[33] G. Legnani, M. Tiboni, Optimal design and application of a low-cost wire-sensor system for the kinematic calibration of industrial manipulators, MAMT 73 (2014) 25–48, http://dx.doi.org/10.1016/j.mechmachtheory.2013.09.005.

[34] M. Goswami, Ambarish, Quaid, Arthur, Peshkin, Complete parameter identification of a robot from partial pose information, in: Proceedings of IEEE Conf. on Control Systems, Vol. 13, No. 5, 1993, pp. 168–173.

[35] A. Nubiola, M. Slamani, I.A. Bonev, A new method for measuring a large set of poses with a single telescoping ballbar, Precis. Eng. 37 (2) (2013) 451–460, http://dx.doi.org/10.1016/j.precisioneng.2012.12.001.

[36] A. Omodei, G. Legnani, R. Adamini, Calibration of a measuring robot: Experimental results on a 5 DOF structure, J. Robot. Syst. 18 (5) (2001) 237–250, http://dx.doi.org/10.1002/rob.1019.

[37] M.R. Driels, Using passive end-point motion constraints to calibrate robot manipulators, J. Dyn. Syst. Meas. Control 115 (3) (1993) 560–566, http://dx.doi.org/10.1115/1.2899139.
[38] D. Bennett, J. Hollerbach, Autonomous calibration of single-loop closed kinematic chains formed by manipulators with passive endpoint constraints, IEEE Trans. Robot. Autom. 7 (5) (1991) 597–606, http://dx.doi.org/10.1109/70.97871.
[39] M. Ikits, J.M. Hollerbach, Kinematic calibration using a plane constraint, in: Proceedings - IEEE International Conference on Robotics and Automation, Vol. 4, No. April, 1997, pp. 3191–3196, http://dx.doi.org/10.1109/robot.1997.606774.
[40] H.N. Nguyen, J. Zhou, H.J. Kang, A new full pose measurement method for robot calibration, Sensors (Basel, Switzerland) 13 (7) (2013) 9132–9147, http://dx.doi.org/10.3390/s130709132.
[41] A. Filion, A. Joubair, A.S. Tahan, I.A. Bonev, Robot calibration using a portable photogrammetry system, Robot. Comput.-Integr. Manuf. 49 (April 2016) (2018) 1339–1351, http://dx.doi.org/10.1016/j.rcim.2017.05.004.
[42] Calibration of parallel robots using two inclinometers, in: Proceedings - IEEE International Conference on Robotics and Automation, Vol. 3, No. May, 1999, pp. 1758–1763.
[43] W.-Y. Chung, Mobility analysis of RSSR mechanisms by working volume, J. Mech. Des. 127 (1) (2005) 156–159, http://dx.doi.org/10.1115/1.1825045.
[44] W.-Y. Chung, Mobility analysis of RSSR linkage and type maps of special cases, Mech. Mach. Theory 39 (4) (2004) 379–393, http://dx.doi.org/10.1016/j.mechmachtheory.2003.09.004.
[45] D. Lee, Y. Youm, W. Chung, Mobility analysis of spatial 4- and 5-link mechanisms of the RS class, Mech. Mach. Theory 31 (5) (1996) 673–690, http://dx.doi.org/10.1016/0094-114X(95)00099-K.
[46] J. Duffy, M. Gilmartin, Displacement analysis of the generalised RSSR mechanism, Mech. Mach. Theory 13 (5) (1978) 533–541, http://dx.doi.org/10.1016/0094-114X(78)90006-X.
[47] R.I. Alizade, G.N. Sandor, Determination of the condition of existence of complete crank rotation and of the instantaneous efficiency of spatial four-bar mechanisms, Mech. Mach. Theory 20 (3) (1985) 155–163, http://dx.doi.org/10.1016/0094-114X(85)90001-1.
[48] W. Zhang, D. Zhang, Conditions of crank existence for a particular case of the rssr linkage, Mech. Mach. Theory 28 (6) (1993) 845–850, http://dx.doi.org/10.1016/0094-114X(93)90027-S.
[49] Z. Saka, The RSSR mechanism with partially constant transmission angle, Mech. Mach. Theory 31 (6) (1996) 763–769.
[50] B. Devanathan, A. Soni, M. Siddhanty, Higher-order synthesis of an RSSR mechanism with application, Mech. Mach. Theory 19 (1) (1984) 85–96, http://dx.doi.org/10.1016/0094-114X(84)90010-7.
[51] K. Lakshminarayana, L. Balaji Rao, Graphical synthesis of the RSSR crank-rocker mechanism, Mech. Mach. Theory 19 (3) (1984) 331–336, http://dx.doi.org/10.1016/0094-114X(84)90067-3.
[52] K. Lakshminarayana, L. Balaji Rao, Optimal designs of the RSSR crank-rocker mechanism—II. Unit time ratio and limits of capability, Mech. Mach. Theory 19 (4) (1984) 443–447, http://dx.doi.org/10.1016/0094-114X(84)90103-4.
[53] K. Gupta, S. Kazerounian, Synthesis of fully rotatable R-S-S-R linkages, Mech. Mach. Theory 18 (3) (1983) 199–205, http://dx.doi.org/10.1016/0094-114X(83)90090-3.
[54] K. Farhang, V. Ghatti, J.M. Cabradilla, Design of harmonic motion generating RSSR four bar mechanisms for high speed application, in: International Design Engineering Technical Conferences and Computers and Information in Engineering Conference, Volume 2: 28th Biennial Mechanisms and Robotics Conference, Parts A and B, 2004, pp. 1427–1434, http://dx.doi.org/10.1115/DETC2004-57559.